Adaptive Binding of Alkyl Glycosides by Nonpeptidic Helix Bundles in Water: Toward Artificial Glycolipid Binding Proteins

Sung Hyun Yoo, Jérémie Buratto, Arup Roy, Estelle Morvan, Morgane Pasco, Karolina Pulka-Ziach, Caterina Lombardo, Frédéric Rosu, Valérie Gabelica, Cameron Mackereth, et al.

Adaptive Binding of Alkyl Glycosides by Non-peptidic Helix Bundles in Water: Toward Artificial Glycolipid Binding Proteins

Sung Hyun Yoo,[a] Jérémie Buratto,[a] Arup Roy,[a] Estelle Morvan,[b] Morgane Pasco,[a] Karolina Pulka-Ziach,[c] Caterina M. Lombardo,[a] Frédéric Rosu,[b] Valérie Gabelica,[b,d] Cameron D. Mackereth,[d] Gavin W. Collie,[e] Gilles Guichard*[,a]

[a]Univ. Bordeaux, CNRS, Bordeaux INP, CBMN, UMR5248, IECB, 2 rue Robert Escarpit, F-33600, Pessac, France

[b]Univ. Bordeaux, CNRS, INSERM, IECB, UAR3033, US001, F-33600, Pessac, France

[c]University of Warsaw, Faculty of Chemistry, Pasteura 1, 02-093, Warsaw, Poland

[d]Univ. Bordeaux, CNRS, INSERM, ARNA, UMR5320, U1212, IECB, F-33600 Bordeaux, France

[e]Discovery Sciences, R&D, AstraZeneca, Cambridge, UK

ABSTRACT: Amphipathic water-soluble helices formed from synthetic peptides or foldamers are promising building blocks for the creation of self-assembled architectures with non-natural shapes and functions. While rationally designed artificial quaternary structures such as helix bundles have been shown to contain preformed cavities suitable for guest binding, there are no examples of adaptive binding of guest molecules by such assemblies in aqueous conditions. We have previously reported a foldamer 6-helix bundle that contains an internal non-polar cavity able to bind primary alcohols as guest molecules. Here, we show that this 6-helix bundle can also interact with larger, more complex guests such as *n*-alkyl glycosides. X-ray diffraction analysis of co-crystals using a diverse set of guests together with solution and gas-phase studies reveal an adaptive binding mode whereby the apo form of the 6-helix bundle undergoes substantial conformational change to accommodate the hydrocarbon chain in a manner reminiscent of glycolipid transfer proteins in which the cavity forms upon lipid uptake. The dynamic nature of the self-assembling and molecular recognition processes reported here marks a step forward in the design of functional proteomimetic molecular assemblies.

INTRODUCTION

Lipids and molecules containing long hydrocarbon chains are essential biomolecules that play unique structural and functional roles in biological systems, *i.e.* as building blocks of cellular compartments, for energy storage and as key signaling molecules[1-3]. Due to their role in these important biological processes, the specific recognition, sensing and transport of long hydrocarbon and lipid chains by dedicated receptor proteins[4] are vital to all living organisms. These processes have inspired the design of synthetic molecular and supramolecular architectures of different shapes intended to similarly bind linear hydrocarbon chains in water. However, the conformational flexibility and lack of distinct recognition site along hydrocarbon chains make the design principles of such receptors difficult to delineate. Nevertheless, diverse receptors ranging from synthetic cavitands, nanocapsules and pores[5-12] to *de novo* peptide assemblies[13,14] exploiting hydrophobic effects or CH-π interactions have been reported to bind hydrocarbon chains in water. Despite notable advances, such as the recent design of polyaromatic receptors with remarkable selectivity for mono-unsaturated fatty acids[10], artificial receptors do not yet compare favorably with natural systems[15-17] in terms of diversity, complexity, selectivity, and adaptability.

A survey of protein structures deposited in the Protein Data Bank (PDB) bound by ligands containing hydrocarbon chains indicates the prevalence of α-helices among secondary structures lining the binding pockets of such proteins[4]. Hydrocarbon binding sites in a number of lipid-binding proteins (LBPs) and lipid transfer proteins (LTPs) are composed of several amphipathic helices arranged/packed in such a way as to create a hydrophobic cavity that can accommodate one or more linear hydrocarbon chains. These cavities may be persistent (*e.g.* albumin superfamily, plant LTPs)

if, for example, the fold is stabilized by interhelical disulfide bridges, or latent, if the cavity does not exist inherently in the apo state of the protein, but transforms following subtle conformational changes upon ligand uptake[16]. Such an adaptive binding mode is a characteristic of glycolipid transfer proteins (GLTPs)[18]. Glycolipid recognition by the saccharide head group recognition site at the surface of GLTPs is coupled to the formation or modification of the hydrophobic pocket resulting in exquisite accommodation of the ligand hydrocarbon chain. The reorganized hydrophobic interaction network and additional hydrogen bonds upon ligand binding thus overcome the conformational transition penalty from apo-GLTP (free state) to holo-GLTP (ligand-bound state). These design features revealed by studies of helical LBPs/LTPs suggested to us that, similarly, aqueous assemblies of non-natural amphipathic helically folded molecules (i.e. foldamers) could behave adaptively and promote the formation of hydrophobic compartments suitable to accommodate hydrocarbon chains bearing a polar head group (e.g. sugar).

Foldamers[19-21], bioinspired synthetic folded oligomers, have emerged as prospective scaffolds to mimic the shapes and functions of biopolymers. The attributes of such foldamer building blocks to create biomimetic architectures are (1) a range of well-defined secondary structure elements including helices of different shapes accessible from the existing (biotic[22-27] or abiotic[28-30]) backbone repertoire, (2) sequence programmability, and (3) a large pool of monomeric units enabling the introduction of side chains equipped with diverse functions (proteinogenic and beyond). More complex synthetic proteomimetic architectures[31] reaching the size of small proteins become accessible by bringing together multiple secondary structure elements in a single strand (foldamer tertiary structure[32-34]) or by self-assembling amphipathic sequences in aqueous environment (foldamer quaternary structure[35-37]). In terms of function, foldamer-based receptors[38-41] have been reported, showing exquisite ligand-specificity that can be modulated by sequence design. In most cases, however, such receptors are restricted to secondary structures and contain a "predictable" pre-existing and unalterable cavity as the ligand binding pocket.

In this report, we show that water-soluble oligourea foldamer quaternary structures can cooperatively and adaptively bind glycolipid-type amphipathic guest molecules consisting of a saccharide head group and a linear hydrocarbon tail. We have determined several high-resolution crystal structures of such foldamer-based receptors in complex with an array of *n*-alkyl glycosides. These structures reveal a common adaptive binding mode whereby the apo form of the bundle undergoes substantial shape change to accommodate the hydrocarbon chain of the ligand in a manner reminiscent of GLTPs. These observations were further corroborated in solution by NMR experiments in the presence of a ligand with a perfluoroalkyl chain and by CD (circular dichroism) using two receptor analogues (a silent mutant and a loss-of-function mutant) and a selection of ligands varying in the length of their hydrocarbon chain and the nature of the sugar group. Together, these results represent a step further toward the design of functional foldamer assemblies for protein mimicry.

RESULTS AND DISCUSSION

Oligourea 6-helix bundle rearranges to bind glycolipid-type detergents. Oligoureas are peptidomimetic foldamers with a urea linkage in place of the peptide bond within their backbone (Fig. 1a), that adopt stable helices akin to α-helices of natural peptides (Fig. 1b). Amphipathic oligourea helices self-assemble in water into a diverse set of quaternary structures modulated by sequence design[37,42,43]. Among these, **H1** self-assembles into a 6-helix bundle whose interior is formed by the sequestration of hydrophobic Leu-type side chains (labeled as Leu^u or L^u hereafter), with a charged and hydrated exterior (Fig. 1b and c)[37]. This bundle is not tightly packed and contains a C_3 symmetric hydrophobic cavity with a volume of ~495 Å^3 that could be used to encapsulate guest molecules such as alkanols. Almost full occupancy was observed for pentanol and hexanol[40]. To test whether this self-assembled system is flexible and dynamic enough to adapt to the nature of the guest and whether larger amphipathic molecules could template new helix assemblies, we decided to employ molecules with longer hydrocarbon chains such as alkyl glycoside detergents as potential guests.

We performed a crystallization screen of **H1** in the presence of a selection of non-ionic detergents and in a few cases obtained co-crystals of interest. Crystallographic analysis of an **H1** crystal (resolution: 1.7 Å) grown in aqueous conditions containing *n*-octyl β-D-glucopyranoside (OGP), a simple synthetic glycolipid-type detergent with four hydroxyl groups and an octyl tail, revealed the formation of a complex (termed **H1**-OGP) composed of an **H1** 6-helix bundle receptor containing six OGP ligands (Fig. 1d). The 6-helix bundle of the **H1**-OGP complex shows a similar overall mode of packing/arrangement of canonical oligourea helices as seen in the apo-**H1** (*i.e.* the **H1** 6-helix bundle in the absence of a guest) previously

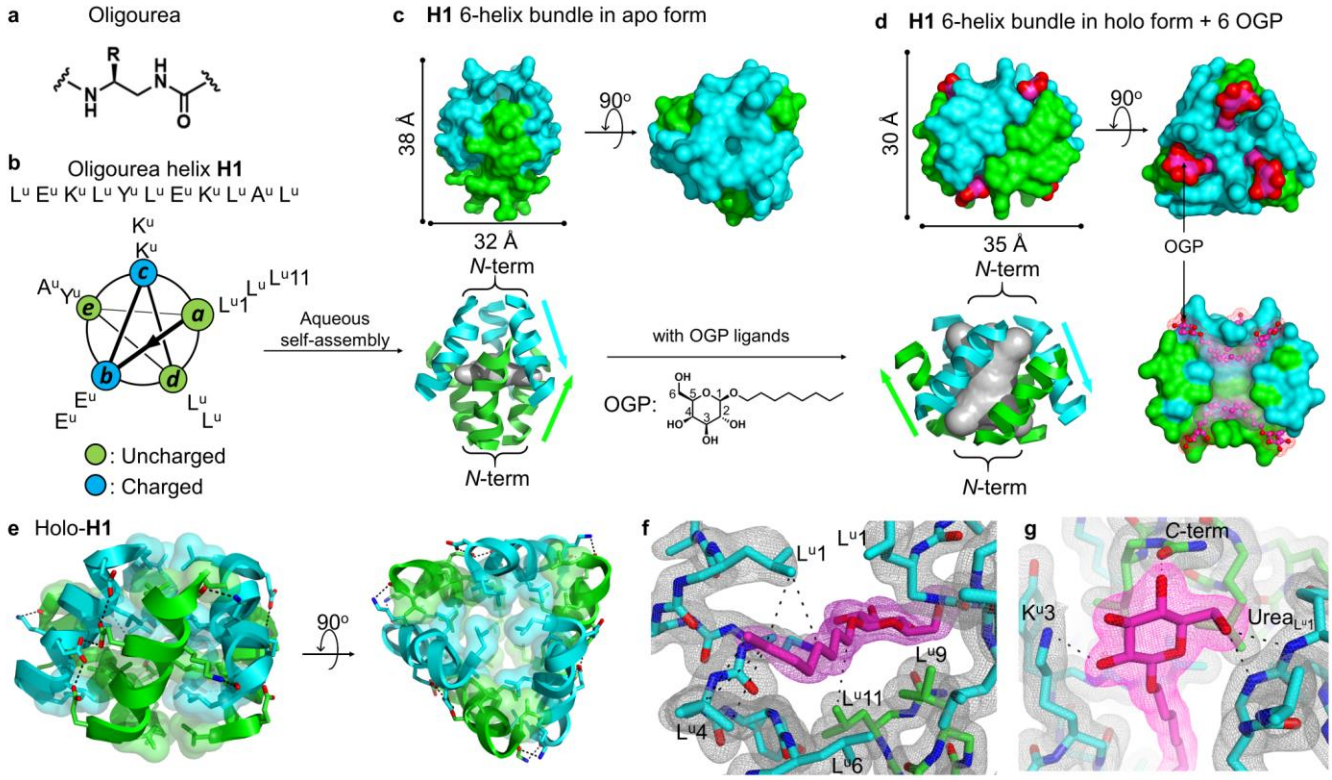

Figure 1. Oligourea **H1** 6-helix bundle rearranges to bind six glycolipid-type detergent ligands. **a**, Chemical structure of oligourea motif. **b**, Sequence of amphiphilic oligourea helix **H1** and its pentad repeat structure. **c**, Crystal structure of **H1** 6-helix bundle (*i.e.* apo-**H1**)[37]. **d**, Crystal structure of **H1** 6-helix bundle bound by six octyl glucopyranoside molecules (OGP, colored in magenta) (*i.e.* **H1**-OGP complex). **H1** helices are colored cyan or green according to the common chain orientation. Hydrophobic cavities excluding ligands are depicted as grey surface models. In **d**, bottom right, a sliced image of the **H1**-OGP complex to clarify the interior structure is shown. **e**, Crystal structure of **H1** in holo form showing hydrophobic Leu^u side chains (sticks plus surface) and inter-helix hydrogen bonds (black dashes). **f**, **g**, Electron density map ($2mF_o$-DF_c) at σ level of 1.0 of **H1**-OGP complex: **f,** focused on the OGP hydrocarbon tail in the hydrophobic Leu^u-rich tunnel and **g**, focused on the OGP glucose headgroup, with details of H-bond interactions with **H1**. Black dashes represent hydrophobic contacts (carbon-carbon distance no longer than 4.1 Å) and intermolecular hydrogen bonds in **f** and **g**, respectively.

described[37] (Fig. 1e and Supplementary Fig. S2). As apo-**H1**, the bundle of holo-**H1** (ligand bound form) can be described as three pairs of antiparallel **H1** helices packed together (Supplementary Fig. S2 and video 1) to form a hydrophobic core. The inter-helical interface (within the dimeric units) consists primarily of interlocked hydrophobic Leu^u side chains, in a manner reminiscent of 'knobs-into-holes' (KIH) interactions observed in α-helix bundles[44]. Additional interactions conserved between the two structures include hydrogen bonds between the amine of the Lys^{u}8 side chain and the free carbonyl oxygen of the Ala^{u}10 urea backbone. However, despite these similarities, subtle differences can be found at the interface between the dimeric units (Fig. 1e and Supplementary Fig. S3). In holo-**H1**, the three dimeric units are held together by the interdigitation of hydrophobic side chains of Leu^{u}4 and Leu^{u}9 and the formation of a hydrogen bond chain involving four Glu^u side chains (including a short d(O,O) of 2.62 Å). In contrast, this array of non-covalent interactions is not observed in apo-**H1**. The consequence is that the two bundles substantially differ in their overall shape (Supplementary video 2). When viewed perpendicular to the bundle axis, the holo form of the bundle (**H1**-OGP) appears as a compressed form of apo-**H1,** with a height reduced from 38 Å to 30 Å. View down the helix axis, holo-**H1** displays a truncated triangular shape with well-defined edges.

Another feature associated with the bundle rearrangement upon ligand uptake is the variation of the volume and shape of the internal cavity, which changes from 495 Å^3 in the apo-**H1** bundle**,** to 1792.4 Å^3 in the holo-**H1** bundle. The enlarged cavity in holo-**H1** is lined with Leu^u side chains (Leu^{u}1, Leu^{u}4, Leu^{u}6, Leu^{u}9 and Leu^{u}11) and opens to the

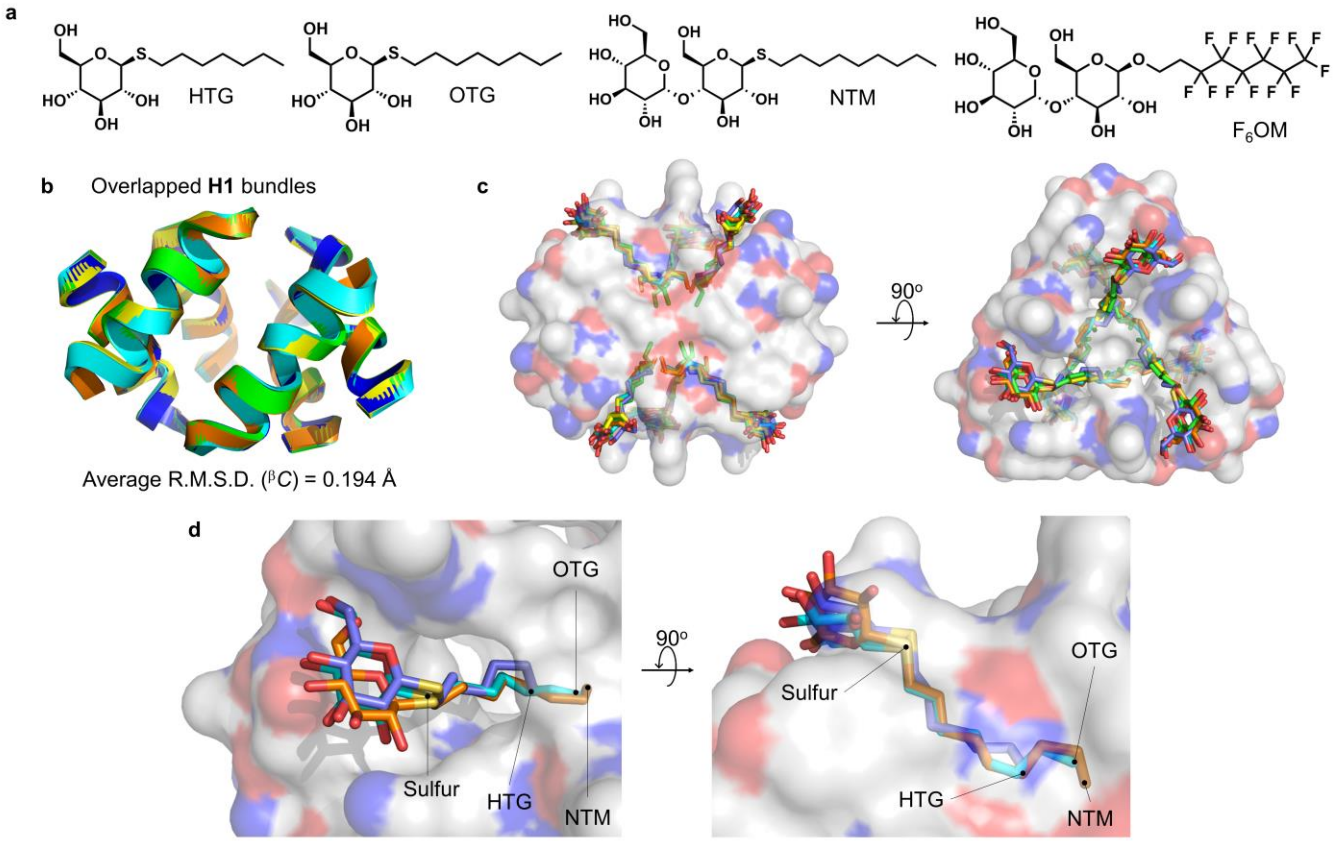

Figure 2. Crystal structures of four additional **H1**-alkyl glycoside complexes. **a**, Chemical structures of alkyl glycosides used as ligands for crystallization with **H1**. **b**, Overlay of **H1** 6-helix bundles from crystal structures of **H1**-ligand complexes. Average $^{\beta}C$ R.M.S.D. is 0.194Å. **c**, Superimposition of all **H1**-ligand complexes with **H1** as a transparent surface model and ligands as stick models (fluorine atoms are omitted for clarity). **d**, Superimposition of **H1** complexes with HTG, OTG and NTM ligands and details showing orientation of the sugar ring at the bundle surface and occupancy of the hydrophobic channel. The thioglycoside sulfur and the terminal carbons of the hydrocarbon chain in HTG, OTG and NTM are labelled for clarity. Helix cartoon in **b** and ligand sticks in **c** and **d** are in different colors to discriminate complexes (**H1**-HTG (blue), **H1**-OGP (yellow), **H1**-OTG (cyan), **H1**-NTM (orange) and **H1**-F_6OM (green)).

exterior of the bundle through six hydrophobic tunnels filled with the hydrocarbon tails (*n*-octyl) of six OGP ligands. The hydrocarbon chains of the OGP molecules are not fully extended, but kinked at the 5th carbon (Supplementary Fig. S4). This kinked conformation, which evokes folding of long hydrocarbon guests in synthetic cages[7], may be a consequence of the close proximity of the six ligands in a confined space. Van der Waals contacts between the hydrocarbon chain and the terminal methyl groups of the Leu^{u} side chains lining the interior of the tunnel are expected to contribute to the binding of OGP (Fig. 1f and Supplementary video 3). In addition, hydrogen bonding between hydroxyl groups of the glucose headgroup and polar moieties at the outer surface of **H1** (i.e. carbohydrate recognition site) are likely to also contribute to the interaction in a manner reminiscent of the recognition of carbohydrate headgroups by GLTPs[16] (Fig. 1g and Supplementary video 3). This hydrogen bonding network is composed of three interactions between (1) the C2-OH of OGP glucose and the amine of the Lys^{u}3 side chain, (2) the C4-OH and the free carbonyl of the *C*-terminal urea and (3) the C6-OH and the urea backbone amine of Leu^{u}1, respectively. Overall, the structure reveals a dual binding mode for OGP involving both van der Waals contacts and hydrogen bonding. The formation of the hydrophobic pocket in response to ligand binding is associated with helix repositioning and the formation of additional contacts between oligourea helices. These stabilizing effects likely compensate for the energy penalty resulting from the conformational transformation of **H1** bundle from the apo to the holo form (Supplementary video 2), which is

strongly reminiscent of human GLTPs that undergo substantial shape change to adaptively accommodate their ligands[16,18].

We then investigated the binding and recognition of other alkyl glycoside detergent ligands by the **H1** bundle by varying the nature of either the polar head group, the hydrocarbon chain or both. Four additional crystals of **H1** complexes were obtained from aqueous solutions of HTG (*n*-heptyl β-D-thioglucopyranoside), OTG (*n*-octyl β-D-thioglucopyranoside), NTM (*n*-nonyl β-D-thiomaltopyranoside) and F_6OM ((1H, 1H, 2H, 2H-perfluorooctyl) β-D-maltopyranoside) (Fig. 2a). X-ray crystallographic structures were successfully determined with resolutions ranging from 1.7 to 2.4 Å (Fig. 2b-d). All five **H1**-detergent complexes are isomorphous, with an average R.M.S.D. (Root Mean Square Deviation) of 0.194 Å calculated for $^{\beta}C$ carbons (the side chain-bearing backbone carbons) of holo-**H1** (Fig. 2b). In each case, the ligand binds into the hydrophobic **H1** bundle cavity in a manner very similar to that previously described for the **H1**-OGP complex (Fig. 2c and Supplementary Fig. S5) with a combination of van der Waals contacts and hydrogen bond interactions between the sugar headgroup and the carbohydrate recognition site. This collection of structures using a small library of ligands suggests that **H1** is capable of binding a range of glycolipid-type molecules with hydrocarbon tails varying in length (from heptyl to nonyl) and composition (hydrocarbon or perfluorinated chain), and with different sugar headgroups (mono- or di-saccharides) and glycosidic bonds (O- or S-). An overlay of the HTG, OTG and NTM ligands in complex with **H1** shows that the sugar rings connected to the hydrocarbon chain interact very similarly with the carbohydrate recognition site of holo-**H1** and superimpose surprisingly well despite the difference in length of the hydrocarbon chains. Overall, the hydrocarbon chains of the three ligands adopt a similar conformation inside the hydrophobic tunnel, with the longer nonyl chain of NTM penetrating deeper into the cavity (Fig. 2d).

Effect of point mutations of H1 on the interaction with alkyl glycosides. We next investigated the effect of specific foldamer sequence variations on the ligand-induced molecular switch from apo-**H1** to holo-**H1** and the concomitant interaction with alkyl glycosides. We designed and prepared two analogues of **H1** containing single residue mutations, namely **H1(E^{u}7N^u)** as a silent mutant and **H1(L^{u}1N^u)** as a loss-of-function mutant, using the same standard oligourea solid phase synthesis procedure as for **H1** (Fig. 3a). The silent mutant **H1(E^{u}7N^u)** has a polar Asn^u replacing Glu^{u}7 residue, a mutation which we predicted to have negligible effect on bundle rearrangement and ligand

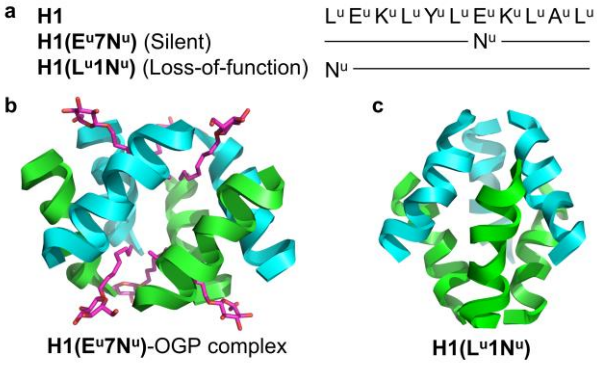

Figure 3. Crystallographic structures of **H1** analogues containing single mutations. **a**, Sequence of **H1**, **H1(E^{u}7N^u)** (silent mutant) and **H1(L^{u}1N^u)** (loss-of-function mutant). **b**, Crystal structure of **H1(E^{u}7N^u)**-OGP complex. **c**, Crystal structure of **H1(L^{u}1N^u)** bundle in apo form from an aqueous CTAB solution.

binding. Crystallographic analysis (resolution: 2.3 Å) revealed **H1(E^{u}7N^u)** to form a 6-helix bundle very similar to holo-**H1** (R.M.S.D. ($^{\beta}C$) = 0. 298 Å) and also bind six OGP molecules (Fig. 3b and Supplementary Fig. S6-S7). As a consequence of the replacement of Glu^u → Asn^u, the hydrogen bond chain that connects **H1** helix dimers is interrupted with the loss of the interhelical H-bonds between the residues in position 7, but the reciprocal hydrogen bonds between the 2nd and 7th urea side chains (Glu^{u}2-Asn^{u}7 for **H1(E^{u}7N^u)**) are retained (Supplementary Fig. S3). The binding characteristics of OGP within the **H1(E^{u}7N^u)**-OGP complex are similar to those found in **H1**-OGP complex, with the six hydrocarbon chains making van der Waals contacts inside the hydrophobic tunnels and the glucose headgroups positioned at the surface of the bundle through a network of three H-bonds (Supplementary Fig. S7).

In the loss-of-function mutant **H1(L^{u}1N^u)**, the hydrophobic Leu^{u}1, whose side chain methyl group is in close proximity with the hydrocarbon tail (intermolecular carbon-carbon distances < 4 Å) in all **H1**-alkyl glycoside complexes, and serves as an entrance gate of the Leu^u-rich tunnel is replaced by a polar Asn^u residue. Therefore, the absence of this key hydrophobic contact in **H1(L^{u}1N^u)** should weaken the interaction of the hydrocarbon chain within the cavity. Despite several crystallization screening campaigns in the presence of a wide range of detergent molecules, we could not co-crystallize **H1(L^{u}1N^u)** with any guest molecule, and only crystals of an apo-**H1(L^{u}1N^u)** 6-helix bundle, whose structure is isomorphous with the apo-**H1** bundle, were obtained from an aqueous solution containing a cationic detergent (CTAB (Cetyltrimethylammonium bromide)) (Fig. 3c and

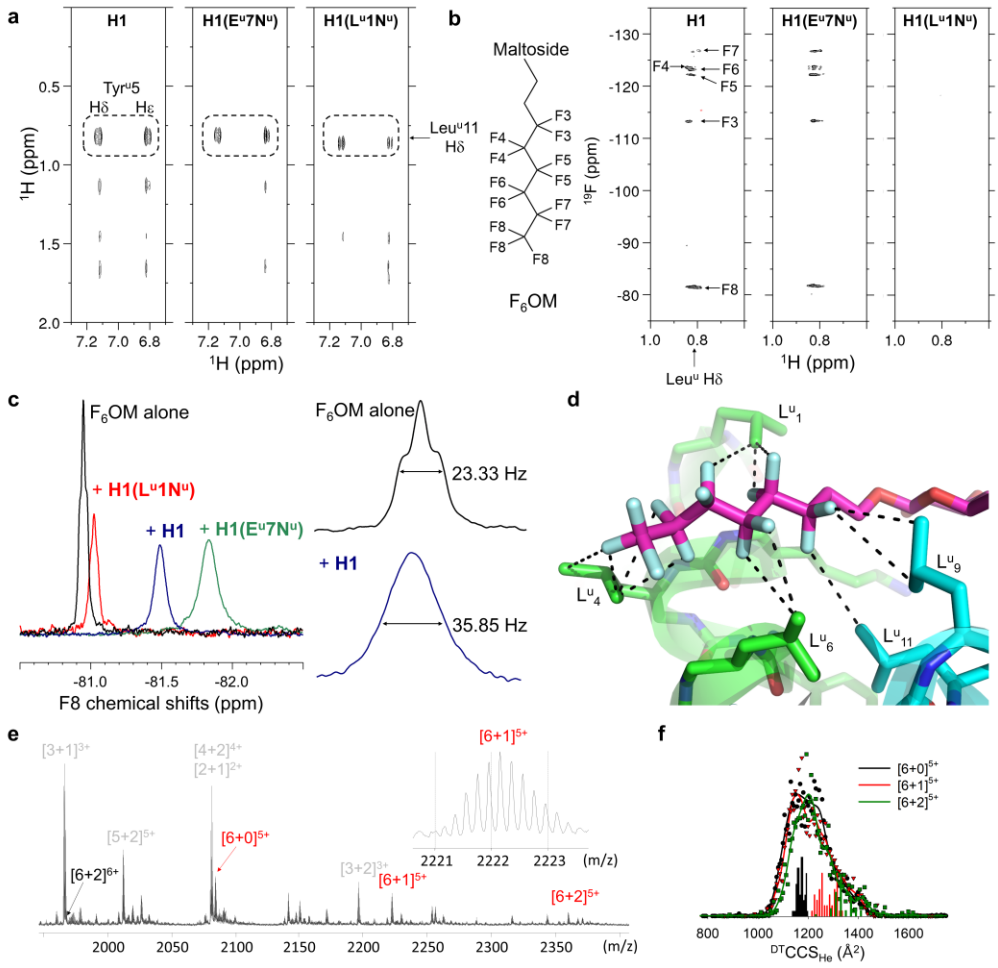

Figure 4. Biophysical analysis of the interaction between **H1** and its analogues with F6OM. **a**, ^{1}H-^{1}H NOESY, **b**, ^{1}H-^{19}F HOESY and **c**, ^{19}F (corresponds to F8 of F6OM) NMR spectra of oligourea bundles (**H1**, **H1(E^{u}7N^{u})** and **H1(L^{u}1N^{u})**) in the presence of F6OM (solution composition: 500 μM foldamer, 500 μM F6OM, 20 mM sodium acetate buffered at pH 4.0 in 98% D_2O solution). Dashed boxes in **a** highlight the NOE signals between Tyr^{u}5 protons (Hδ and Hε) and Leu^{u}11 Hδ, a signature of inter-helix proximity characteristic of bundle formation. Heteronuclear NOE signals are observed between all fluorine atoms of F6OM and Leu^{u} Hδ of **H1** and **H1(E^{u}7N^{u})**, whereas no heteronuclear NOE signal is obtained with **H1(L^{u}1N^{u})** (experimental parameters for each ^{1}H-^{19}F HOESY are identical: 800 ms mixing time and 256 scans). **d**, Crystal structure of **H1**-F6OM complex showing spatial proximity between fluorine atoms (bright cyan) and Leu^{u} Hδs. Dashed lines represent C-F distances ≤ 4.3 Å. **e**, Native ESI-MS analysis of **H1** in the presence of F6OM shows the presence of various **H1**-F6OM complexes, recorded from aqueous solutions containing 100 μM **H1**, 100 μM F6OM and 20 mM ammonium acetate. Corresponding $[m+n]^{z+}$ (m= number of **H1**, n=number of F6OM) are noted above peaks. The isotopic distribution at m/z = 2222.1 with an isotope spacing of 0.2 m/z (inset) unambiguously corresponds to $[6+1]^{5+}$. **f**, Collision cross section ($^{DT}CCS_{He}$) distributions of the $[6+0]^{5+}$ (black, circle), $[6+1]^{5+}$ (red, triangle) and $[6+2]^{5+}$ (green, square) species measured by drift tube ion mobility ESI-MS. The corresponding theoretical CCS distributions are displayed as histograms using the crystal structures as starting models.

Supplementary Fig. S6). Although not proving definitively that **H1(L^{u}1N^{u})** cannot bind any detergent molecule, these results and crystal structures nevertheless support the hypothesis that the hydrophobicity at the entrance of the tunnel is required in order for detergents to bind and stabilize the bundle-ligand complex.

Biophysical analysis of the receptor-ligand complexes. With high-resolution structures of oligourea foldamer bundle-alkyl glycoside complexes in hand, we turned to NMR and native electrospray ionization mass spectrometry (native ESI-MS) to study the interaction between the foldamer receptor and its ligands in both solution and gas phases. We chose F6OM as a model ligand, as its perfluorinated chain would allow us to discriminate between the NMR signals of Leu^{u} residues lining the hydrophobic tunnel and those from the ligand, and

thus to identify through-space interactions between the foldamer bundle and the ligand using homo- and heteronuclear multidimensional NMR experiments.

First, ^{1}H-^{1}H NOESY NMR spectra of **H1** and its two analogues (**H1(E^{u}7N^{u})** and **H1(L^{u}1N^{u})**) in the presence of F_6OM in aqueous solutions clearly showed NOE signals between Tyr^{u}5 side chain protons (Hδ and Hε) and Leu^{u}11 side chain -CH_3 protons (Hδ) (Figure 4a) (experimental parameters for each ^{1}H-^{1}H NOESY are identical: 300 ms of mixing time and 256 scans at 25 °C). These NOE signals between two residues remote from each other in an isolated foldamer helix were shown previously to indicate inter-helix proximity and were considered as a fingerprint for bundle formation by **H1** and its analogues[37,42-45]. Examination of the crystal structures of the **H1** bundle-alkyl glycoside complexes suggests that these NOE signals are also compatible with the holo-form of **H1** bundle (Supplementary Fig. S8). Although it is not possible to differentiate between the apo- and holoforms of **H1** by these NOE signals, their observation supports the propensity of all three **H1** analogues to form bundles in aqueous conditions in the presence of F_6OM.

^{1}H-^{19}F HOESY (heteronuclear NOESY) NMR spectra of the three abovementioned samples recorded under the same NMR experimental parameters (800 ms of mixing time and 256 scans at 25 °C) showed different heteronuclear NOE signals (Fig. 4b). In the presence of **H1** (or the silent mutant **H1(E^{u}7N^{u})**), heteronuclear NOE signals are observed between all fluorine atoms of F_6OM with the foldamer Leu^{u} side chain –CH_3 protons (Hδ). These signals confirm that the fluorocarbon tail is spatially close to the Leu^{u} residues lining the tunnel of the bundles, and is consistent with the crystal structure of **H1**-F_6OM complex (Fig. 4d). In contrast, no equivalent heteronuclear NOE signal was observed in the case of the loss-of-function mutant **H1(L^{u}1N^{u})**, demonstrating that this **H1** analogue is not able to interact with the carbon chain of the ligand (or at least with binding that is too weak to be detected by NMR). In addition, ^{19}F NMR analysis of the three samples shows that the chemical shift and shape of the ^{19}F peaks of the ligand differ with the foldamer receptor. In the presence of **H1** (or **H1(E^{u}7N^{u})**), the chemical shifts of ^{19}F atoms in F_6OM are clearly shifted, whereas only a tiny shift was obtained in the presence of **H1(L^{u}1N^{u})** (Fig. 4c and Supplementary Fig. S9 and Table S3). Fast exchange between the free and the bound state of the ligand occurred on the NMR time scale thus only one average signal is observed on the spectrum, but significant peak broadening in **H1** and **H1(E^{u}7N^{u})** samples confirms binding events taking place (Fig. 4c and Supplementary Fig. S10 and Table S4). Overall, 1D and 2D NMR spectra are consistent with **H1** and **H1(E^{u}7^{u}N)** binding to the F_6OM tail in aqueous solution, and with **H1(L^{u}1N^{u})** having no such (or much less) interaction with the F_6OM hydrocarbon tail.

Native ESI-MS analysis of the three foldamers in the presence of F_6OM revealed the presence of several complexes composed of multimeric foldamers plus F_6OM, but foldamer sequence-dependent ligand binding was not observed (Fig. 4e and Supplementary Fig. S11). Although there is no predominant complex species, it is notable that the receptor-ligand interaction is strong enough such that complex species are detectable following ionization. To investigate whether the ion species of **H1** assemblies ($[6+0]^{5+}$, $[6+1]^{5+}$ and $[6+2]^{5+}$) found in MS can correspond to the crystal structures of **H1** bundles, ion mobility-mass spectrometry (IM-MS) was used in concert with semi-empirical (PM7)[46] calculations, Atom-centered Density Matrix Propagation (ADMP) molecular dynamics and trajectory model[47] collision cross section calculations.

IM-MS analysis revealed that the experimental collision cross section (CCS) distributions in helium for **H1**-F_6OM complexes ($[6+1]^{5+}$ and $[6+2]^{5+}$) are from 1000 to 1400 Å^2, the same range obtained for CCS distribution of apo-**H1** ($[6+0]^{5+}$) (Fig. 4f and Supplementary Fig. S12). This suggests that the size and shape of the three ion species are similar regardless of F_6OM binding, which implies F_6OM being captured inside of the assemblies. However, the high-CCS tail is relatively more abundant for the complexes. Theoretical CCSs were calculated for three gas-phase structures ($[6+0]^{5+}$, $[6+1]^{5+}$ and $[6+2]^{5+}$) built from the crystal structures of apo-**H1** bundle (1260 Å^2) and **H1**-F_6OM complexes (hexameric bundle plus six F_6OM) (1336 Å^2) as starting models. Theoretical CCSs are within the experimental CCS profiles. The main peak centered around 1200 Å^2 matches well with the apo structure, while the tails are in line with the holo form. Note however that the complexes observed from dilute solutions by IM-MS contain fewer ligands (1 or 2) than the crystal structure (6 ligands), and a collapse of the cavities in the gas phase is not surprising. The overlaps of experimental and theoretical CCS profiles support that structures of the three ion species are compatible with the crystal structures of **H1** bundle end-products.

Overall, the biophysical analyses using NMR, native mass spectrometry and ion mobility support a model of interaction between the foldamer bundle receptor and the alkyl glycoside ligand in

Table 1. Crystallographic analysis and biophysical analysis (based on CD-monitored data) of the foldamer bundle-glycolipid guest complexes.

Receptor	Ligand	Surface area of hydrophobic tail[a] (Å²)	Biophysical analysis (CD-monitored data)		
			% increase in folding[b]	Temperature-dependent	
				$T_{1/2}$(°C)[c]	adj. R^2
H1			-	41.5[d]	0.9988[d]
H1	HTG	261.0	12	39.9	0.9623
H1	OTG	300.0	17	42.1	0.9656
H1	OGP	302.3	19	47.1	0.9813
H1	NTM	333.7	56	50.8	0.9920
H1	F_6OM	356.2	76	87.3	0.9957
H1(E^u7N^u)			-	30.0	0.9758
H1(E^u7N^u)	OGP	303.5	9	50.6	0.9775
H1(E^u7N^u)	F_6OM		74	81.7	0.9942
H1(L^u1N^u)			-		
H1(L^u1N^u)	F_6OM		32	54.1	0.9885

[a]Solvent-accessible surface areas (SASA) of hydrophobic tails (oxygen and sulfur atoms were excluded, thus only the alkyl tails were considered) were calculated using the get_area function in PyMOL using a 1.4 Å probe radius. For precise comparison, protons of hydrocarbon tails were generated using the h_add function in PyMOL. Receptors and neighboring five ligands were removed to calculate SASA of each ligand. [b]% increase in folding values (% increase of MRE_{204} of interest versus MRE_{204} of reference (i.e. MRE_{204} of receptor alone)) at a ligand concentration of 2 mM and receptor concentration of 0.2 mM. [c]The mid-point of the transition ($T_{1/2}$) values were estimated by fitting temperature-dependent CD data to a simple two-state Boltzmann unfolding model using OriginPro 9.0. [d]$T_{1/2}$ of apo-**H1** is from reference[40]. Note that $T_{1/2}$ of **H1(L^u1N^u)** could not be determined.

which the linear alkyl chain is buried within a hydrophobic pocket, which is in-line with our crystallographic observations.

Ligand-dependent binding affinity and complex stability. The characterization at high resolution of the receptor complexes with various ligands and the evidence that recognition of alkyl glycosides might also occur in solution encouraged us to investigate these interactions in more detail with a focus on how these interactions may vary with the nature of the ligand. To facilitate the comparison of the ligands which differ by both the length (C7 to C9) and composition (alkyl and fluoroalkyl chain) of their hydrophobic tail, we calculated the corresponding solvent-accessible surface area (SASA) of these ligands. Previous studies have shown that free energy of interaction of alkyl and fluoroalkyl chains with a protein surface correlates well with their SASA[48]. The average values of SASA of the hydrophobic tails of the ligands co-crystallized with **H1** are reported in Table 1 and reveal the following ranking: F_6OM>NTM>OGP≈OTG>HTG. Thus, the hydrophobic effect of the F_6OM tail would be the strongest and that of the HTG tail would be the weakest. The receptor-ligand interactions were then investigated in water by monitoring helicity as a measure of bundle stability using circular dichroism (CD) (Table 1 and Fig. 5). We first measured CD spectra of foldamers (**H1**, **H1(E^u7N^u)** and **H1(L^u1N^u)**) at a concentration of 200 μM plus glycolipid-type detergents at a concentration of 2 mM (10 molar equivalents to foldamer) in pure water (Fig. 5a and Supplementary Fig. S13). All CD spectra were recorded over a wavelength range of 190 – 250 nm and showed λ_{max} around 204 nm, which is a characteristic of the canonical oligourea helix conformation. This is consistent with the crystallographic structures showing that the presence of ligand does not alter

the helical structure of oligourea foldamers. The value of the molar residual ellipticity (MRE, deg·cm^2·dmol^{-1}·residue^{-1}) at 204 nm (MRE_{204}), which indicates helical stability (also, indirectly, bundle stability) of oligourea foldamers, increased when **H1** is in the presence of the detergents and this increment is different depending on the nature of the ligand (Fig. 5a). For numerical comparisons, we used % increase in folding values, which correspond to % increase of the MRE_{204} value of interest versus the MRE_{204} value of the reference (i.e. apo-bundle). % increase in folding of **H1** increased from 12% to 56%, as ligands changed from HTG to NTM, respectively, i.e. with increasing hydrocarbon length (and SASA) of ligands. The highest value of 76% was obtained with F_6OM (bearing a fluorinated carbon chain). The trend in ligand-dependent helix stability of foldamers supports our expectation that the hydrophobic effect may drive the stability of the receptor-ligand complexes.

We also conducted temperature-dependent CD-experiments to investigate the receptor-ligand complex stability as a function of the nature of the ligand. Temperature-dependent MRE_{204} values of each foldamer-ligand combination (at the same concentration as abovementioned CD analysis) were recorded upon heating from 4 °C to 90 °C with a heating rate of 1 °C/minute. Although these data may not reflect a simple two-state equilibrium but a more complex system, the mid-point of the transition ($T_{1/2}$) is a useful indicator for helix unfolding and bundle disassembly which can be used to compare receptor-ligand complexes (Fig. 5b and Supplementary Fig. S14). $T_{1/2}$ values determined from these temperature-dependent data were shown to vary depending on the nature of the alkyl glycoside ligands. For instance, both NTM and F_6OM significantly increase the $T_{1/2}$ of **H1** by 9.3 °C and 45.8 °C, respectively, while HTG has negligible effect on the $T_{1/2}$ of **H1**. The ligand-dependent $T_{1/2}$ and MRE_{204} value increases are directly correlated with the SASA of ligand tails. Concurrently, we performed the same experiments with the two **H1** mutants to investigate in more detail how sequence variations may affect ligand recognition. The % increase in folding (74% and 32%) and $T_{1/2}$ (81.7 °C and 54.1 °C) values obtained for **H1(E^{u}7N^u)** and **H1(L^{u}1N^u)**, respectively in the presence of F_6OM indicate clear differences in the behavior of the two mutants. Whereas **H1(E^{u}7N^u)** shows values very similar to those measured with **H1**, the values recorded for the loss-of-function mutant (**H1(L^{u}1N^u)**) are substantially reduced. This is consistent with NMR data and supports the view that **H1(L^{u}1N^u)** has a reduced ability to bind (fluoro)alkyl glycosides as a result of the lower hydrophobicity of the Leu^u-rich tunnel.

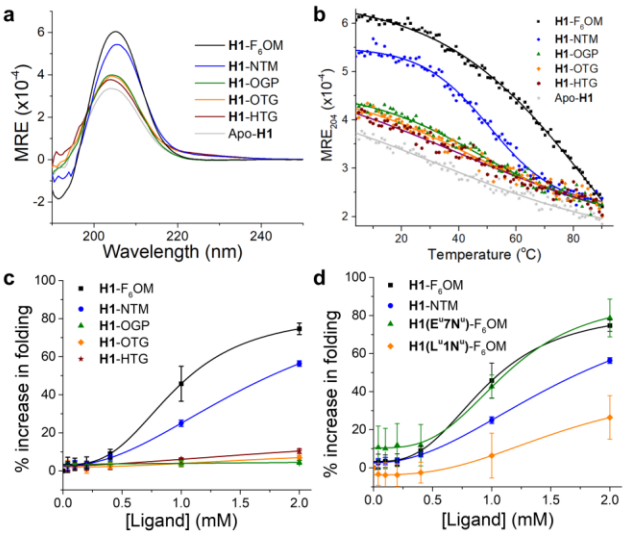

Figure 5. CD-monitored biophysical analysis of foldamer bundle receptor-ligand complexes. **a**, CD spectra and **b**, Temperature-dependent CD experiments with [**H1**] = 200 μM in the absence or presence of ligands ([Ligand] = 2 mM). **c** and **d**, CD-monitored titration of foldamer receptor-ligand complex. Curves represent Hill equation fitting. Error bars represent standard deviation of three experiments.

CD-monitored titration of ligands into foldamer bundles was performed in order to understand foldamer bundle receptor-ligand binding in more detail. Ligand solutions were sequentially added to a 200 μM foldamer solution to vary the molar ratio ([ligand]:[foldamer]) from 5:1 to 1: 10 and % increase in folding values at each molar ratio were recorded. Unlike HTG, OTG and OGP whose addition showed only a limited effect on the CD signal, the titration with NTM and F_6OM led to a sigmoidal increase of the % increase in folding values (Fig. 5c and Supplementary Fig. S15). The sigmoidal increment was also observed when F_6OM was added to the **H1** analogues (Fig. 5d and Supplementary Fig. S16). Hill plot fitting of the CD-monitored titration data revealed a good fit for the four receptor-ligand combinations (**H1**-NTM, **H1**-F_6OM, **H1(E^{u}7N^u)**-F_6OM and **H1(L^{u}1N^u)**-F_6OM) with adj. R^2 values higher than 0.95. The other CD-monitored titration data did not fit well to the Hill equation (adj. R^2 values are lower than 0.9, Supplementary Fig. S15-S16). Although the system is quite complex, we attempted in all four cases to extract $[L]_{1/2}$, which corresponds to the ligand concentration needed to occupy half of the binding sites, by assuming that the receptor state is the 6-helix bundle. The lower $[L]_{1/2}$ value (indicating a higher binding affinity) with F_6OM (0.95 mM) compared to NTM (1.79 mM) is consistent

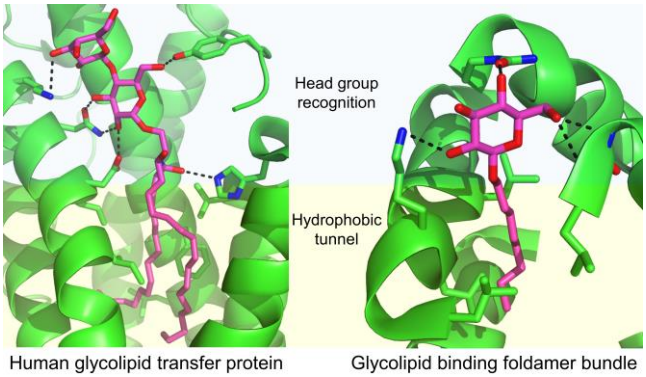

Figure 6. Comparison of crystal structures of a human glycolipid transfer protein (GLTP)/glycosphingolipid complex[18] (left, PDB ID: 1SX6) and urea foldamer bundle/*n*-alkyl glycoside complex (right). Despite apparent differences, the natural and unnatural systems share some common features, such as hydrogen bond mediated head group recognition and a hydrophobic compartment for binding hydrocarbon chains. Helix cartoon represents the protein (or foldamer) and green sticks represent selected residues participating to intermolecular hydrogen bonding (dashed lines) or involved in van der Waals contacts. Guest molecules are shown as magenta sticks.

with the above-mentioned experiments and SASA analysis. Hill coefficients (n) of the four combinations are around 2 ~ 3 (higher than 1, but lower than the number of binding sites (6)), thus suggesting that binding of the ligands within foldamer bundles is moderately cooperative. Considering that the foldamer bundle receptor has six binding sites and that binding events may favor foldamer bundle assembly into the holo form required to bind additional alkyl glycoside molecules, the cooperative binding mode is consistent with structures of the complexes obtained by crystallography.

CONCLUSION

Supramolecular cavities and channels within artificial helix bundles assembled from amphipathic peptide and foldamer helices provide privileged environments for interacting with guest molecules ranging from small organic ligands to lipophilic biologically active molecules[14,40-42,49,50]. High resolution structural studies have revealed cavities differing considerably in shape (e.g. open or closed), volume and interior (polar versus hydrophobic). A common characteristic of the cavities of these systems, besides potential tunability by sequence variation, is that they are generally preformed, i.e. they exist in the apo-state. For example, we have previously shown using X-ray crystallography that the central non-polar cavity formed within the **H1** oligourea 6-helix bundle (empty in the apo-form) can host simple alkanols – with pentanol and hexanol showing the best shape complementarity – and that this binding does not affect the original structure of the bundle[37,40].

Here, by using larger and more challenging guest molecules (i.e. *n*-alkyl glycosides) that cannot fit into this pre-existing cavity, we show that the previously described oligourea 6-helix bundle can rearrange into a closely related yet distinct bundle to accommodate the new guest molecules. Structural studies of co-crystals formed between the oligourea foldamer and various *n*-alkyl glycosides allowed us to precisely identify and characterize guest-mediated rearrangements of the quaternary structure. Remarkably, all the structures show that the hydrophobic compartments that host the hydrocarbon chain of the ligands are not preexisting in the apo-state but actually take shape in the presence of the ligand, revealing adaptability of the system. This is further supported by the temperature-dependent CD profile of **H1** in the presence of NTM (Fig. 5b), for example, which shows a clear increase in thermal stability, with a more pronounced transition indicative of adaptive ligand recognition and cooperativity. This process necessitates concerted movements and repositioning of foldamer helices with the creation of new 'knobs-into-holes' interactions compared to the apo-form. The binding of the ligands involves a combination of van der Waals interactions between the hydrocarbon tail and the hydrophobic interior and a H-bond network between the carbohydrate head groups and the solvent-facing polar oligourea residues. Although this is a purely artificial system formed by a synthetic oligomer quaternary structure and a non-ionic detergent, it is striking how the general ligand binding principles and reorganization of the hydrophobic pocket described here are reminiscent, though at a much simpler level, of human GLTPs (Fig. 6). GLTPs are ubiquitous, highly helical, soluble proteins which by reversibly and non-covalently associating with glycosphingolipids enhance their aqueous solubility and accelerate intermembrane trafficking[16,18]. Although glycosphingolipids are unlikely to be accommodated by the **H1** helix-bundle, the crystal structures reported here nevertheless suggest that the hydrophobic pocket could accommodate long aliphatic chains including perhaps some degree of unsaturation. Comparative analyses of different ligands and the use of foldamer sequences containing single mutations suggest that the complementarity between the Leu^{u}-rich tunnels and the hydrocarbon tails is an important requisite for the binding. Subtle modifications of the hydrophobic compartment using closely related and/or chemically different residues may be a rational

route to modulate shape complementarity and affinity for the hydrocarbon chain and accommodate lipids with longer chains (>C10). Along these lines, our studies of F_6OM, as well as work by others[51,52], suggests that substituting the methyl groups of Leu^u residues within the bundle by trifluoromethyl groups may be a fruitful avenue of investigation to increase binding affinity as high as natural GLTPs (K_D in the μM range)[53]. Furthermore, the polar outer surface of the helix bundle is expected to provide a modular environment to preferentially anchor certain lipid polar head groups via the formation of an optimal H-bond network, allowing, potentially, the design of enhanced lipid binding selectivity, as in LTPs. This could be tested by screening amphiphiles with a wider range of hydrophilic head groups in terms of stereochemistry and composition than those tested here.

Adaptive binding is a key feature of the synthetic system reported here. The changes in size and shape of the hydrophobic pocket from the apo to the holo form of the bundle certainly reflects the intrinsic dynamics of the quaternary structure formed by **H1**[37,43], in which entities of various stoichiometries and shapes may interconvert in a continuous assembly/disassembly process[54]. This dynamic character makes water-soluble amphipathic oligourea helical foldamers promising building blocks to further develop artificial synthetic protein-like assemblies with a diversity of shapes and functions, including as new stimuli-responsive materials.

ASSOCIATED CONTENT

Supporting Information.
Full description of methods for chemistry, X-ray crystallography, NMR spectroscopy, native mass spectrometry and CD spectroscopy procedures; videos of apo-**H1**, holo-**H1** and **H1**-OGP crystal structures; additional figures. This material is available free of charge via the Internet at http://pubs.acs.org.xxx

AUTHOR INFORMATION

Corresponding Author

Gilles Guichard – Univ. Bordeaux, CNRS, Bordeaux INP, CBMN, UMR 5248, Institut Européen de Chimie et Biologie, 2 rue Robert Escarpit, 33607, Pessac, France; https://orcid.org/0000-0002-2584-7502; E-mail: g.guichard@iecb.u-bordeaux.fr

Authors

Sung Hyun Yoo – Univ. Bordeaux, CNRS, Bordeaux INP, CBMN, UMR 5248, IECB, 2 rue Robert Escarpit, 33607, Pessac, France; https://orcid.org/0000-0002-9247-0434

Jérémie Buratto – Univ. Bordeaux, CNRS, Bordeaux INP, CBMN, UMR 5248, IECB, 2 rue Robert Escarpit, 33607, Pessac, France; https://orcid.org/0000-0002-6730-336X

Arup Roy – Univ. Bordeaux, CNRS, Bordeaux INP, CBMN, UMR 5248, IECB, 2 rue Robert Escarpit, 33607, Pessac, France; https://orcid.org/0000-0001-8925-2770

Estelle Morvan – Univ. Bordeaux, CNRS, INSERM, IECB, UAR 3033, 2 rue Robert Escarpit, 33607, Pessac, France; https://orcid.org/0000-0003-4071-7885

Morgane Pasco – Univ. Bordeaux, CNRS, Bordeaux INP, CBMN, UMR 5248, IECB, 2 rue Robert Escarpit, 33607, Pessac, France; https://orcid.org/0000-0002-1556-2802

Karolina Pulka-Ziach – University of Warsaw, Faculty of Chemistry, Pasteura 1, 02-093, Warsaw, Poland; https://orcid.org/0000-0002-2861-1466

Caterina M. Lombardo – Univ. Bordeaux, CNRS, Bordeaux INP, CBMN, UMR 5248, IECB, 2 rue Robert Escarpit, 33607, Pessac, France; https://orcid.org/0000-0001-5644-8187

Frédéric Rosu – Univ. Bordeaux, CNRS, INSERM, IECB, UAR 3033, F-33600 Pessac, France; https://orcid.org/0000-0003-3674-7539

Valérie Gabelica – Univ. Bordeaux, CNRS, INSERM, ARNA, UMR 5320, U1212, IECB, F-33600 Bordeaux, France; https://orcid.org/0000-0001-9496-0165

Cameron D. Mackereth – Univ. Bordeaux, CNRS, INSERM, ARNA, UMR 5320, U1212, IECB, F-33600 Bordeaux, France; https://orcid.org/0000-0002-0776-7947

Gavin W. Collie – *Discovery Sciences, R&D, AstraZeneca, Cambridge, UK;* https://orcid.org/0000-0002-0406-922X

Author Contributions

All authors have given approval to the final version of the manuscript.

Notes

The authors declare no competing financial interest.

ACKNOWLEDGMENT

This work was supported in part by the Agence Nationale de la Recherche (ANR) grants ANR-17-CE07-0020. Post-doctoral fellowships to S.H.Y. from IdEx Bordeaux (ANR-10-IDEX-03-02), a program of the French government managed by the ANR and from ANR-17-CE07-0020 are gratefully acknowledged. A Marie Skłodowska-Curie postdoctoral fellowship (H2020-MSCA-IF-2014, project #661247) to A.R. is also gratefully acknowledged. We thank the SOLEIL and ESRF synchrotrons for providing access to data collection facilities. This work has benefited from the facilities and expertise of IECB Biophysical and Structural Chemistry platform (BPCS), CNRS UAR3033, Inserm US001, Univ. Bordeaux.

REFERENCES

(1) Gunstone, F. D. *Fatty Acid and Lipid Chemistry*; Springer US: Boston, MA, 1996.

(2) Vance, D. E. & Vance, J. E. (eds). *Biochemistry of Lipids, Lipoproteins and Membranes*, 5th ed.; Vance, D. E. & Vance, J. E., Ed.; Elsevier: Amsterdam, 2008.

(3) Huang, Z. R.; Lin, Y. K.; Fang, J. Y. Biological and Pharmacological Activities of Squalene and Related Compounds: Potential Uses in Cosmetic Dermatology. *Molecules* **2009**, *14*, 540–554.

(4) Park, J.; Pham, H. V.; Mogensen, K.; Solling, T. I.; Bennetzen, M. V.; Houk, K. N. Hydrocarbon Binding by Proteins: Structures of Protein Binding Sites for ≥C10 Linear Alkanes or Long-Chain Alkyl and Alkenyl Groups. *J. Org. Chem.* **2015**, *80*, 997–1005.

(5) Schramm, M. P.; Rebek, J. Moving Targets: Recognition of Alkyl Groups. *Chem. Eur. J.* **2006**, *12*, 5924–5933.

(6) Trembleau, L.; Rebek, J. Helical Conformation of Alkanes in a Hydrophobic Cavitand. *Science* **2003**, *301*, 1219–1220.

(7) Gavette, J. V.; Zhang, K. Da; Ajami, D.; Rebek, J. Folded Alkyl Chains in Water-Soluble Capsules and Cavitands. *Org. Biomol. Chem.* **2014**, *12*, 6561–6563.

(8) Gibb, C. L. D.; Gibb, B. C. Templated Assembly of Water-Soluble Nano-Capsules: Inter-Phase Sequestration, Storage, and Separation of Hydrocarbon Gases. *J. Am. Chem. Soc.* **2006**, *128*, 16498–16499.

(9) Yazaki, K.; Sei, Y.; Akita, M.; Yoshizawa, M. A Polyaromatic Molecular Tube that Binds Long Hydrocarbons with High Selectivity. *Nat. Commun.* **2014**, *5*, 5179.

(10) Niki, K.; Tsutsui, T.; Yamashina, M.; Akita, M.; Yoshizawa, M. Recognition and Stabilization of Unsaturated Fatty Acids by a Polyaromatic Receptor. *Angew. Chemie. Int. Ed.* **2020**, *59*, 10489–10492.

(11) Lu, X.; Isaacs, L. Uptake of Hydrocarbons in Aqueous Solution by Encapsulation in Acyclic Cucurbit[*n*]uril-Type Molecular Containers. *Angew. Chemie. Int. Ed.* **2016**, *55*, 8076–8080.

(12) Zhang, D.; Ronson, T. K.; Nitschke, J. R. Functional Capsules via Subcomponent Self-Assembly. *Acc. Chem. Res.* **2018**, *51*, 2423–2436.

(13) Ho, D. N.; Pomroy, N. C.; Cuesta-Seijo, J. A.; Privé, G. G. Crystal Structure of a Self-Assembling Lipopeptide Detergent at 1.20 Å. *Proc. Natl. Acad. Sci. U. S. A.* **2008**, *105*, 12861–12866.

(14) Thomas, F.; Dawson, W. M.; Lang, E. J. M.; Burton, A. J.; Bartlett, G. J.; Rhys, G. G.; Mulholland, A. J.; Woolfson, D. N. De Novo-Designed α-Helical Barrels as Receptors for Small Molecules. *ACS Synth. Biol.* **2018**, *7*, 1808–1816.

(15) Salminen, T. A.; Blomqvist, K.; Edqvist, J. Lipid Transfer Proteins: Classification, Nomenclature, Structure, and Function. *Planta* **2016**, *244*, 971–997.

(16) Malinina, L.; Patel, D. J.; Brown, R. E. How α-Helical Motifs Form Functionally Diverse Lipid-Binding Compartments. *Annu. Rev. Biochem.* **2017**, *86*, 609–636.

(17) Wong, L. H.; Gatta, A. T.; Levine, T. P. Lipid Transfer Proteins: The Lipid Commute via Shuttles, Bridges and Tubes. *Nat. Rev. Mol. Cell Biol.* **2019**, *20*, 85–101.

(18) Malinina, L.; Malakhova, M. L.; Teplov, A.; Brown, R. E.; Patel, D. J. Structural Basis for Glycosphingolipid Transfer Specificity. *Nature* **2004**, *430*, 1048–1053.

(19) Gellman, S. H. Foldamers: A Manifesto. *Acc. Chem. Res.* **1998**, *31*, 173–180.

(20) Hill, D. J.; Mio, M. J.; Prince, R. B.; Hughes, T. S.; Moore, J. S. A Field Guide to Foldamers. *Chem. Rev.* **2001**, *101*, 3893–4011.

(21) Guichard, G.; Huc, I. Synthetic Foldamers. *Chem. Commun.* **2011**, *47*, 5933–5941.

(22) Appella, D. H.; Christianson, L. A.; Klein, D. A.; Powell, D. R.; Huang, X.; Barchi, J. J.; Gellman, S. H. Residue-Based Control of Helix Shape in β-Peptide Oligomers. *Nature* **1997**, *387*, 381–384.

(23) Sawada, T.; Gellman, S. H. Structural Mimicry of the α-Helix in Aqueous Solution with an Isoatomic α/β/γ-Peptide Backbone. *J. Am. Chem. Soc.* **2011**, *133*, 7336–7339.

(24) Seebach, D.; Gardiner, J. Beta-Peptidic Peptidomimetics. *Acc. Chem. Res.* **2008**, *41*, 1366–1375.

(25) Semetey, V.; Rognan, D.; Hemmerlin, C.; Graff, R.; Briand, J. P.; Marraud, M.; Guichard, G. Stable Helical Secondary Structure in Short-Chain *N*,*N*'-Linked Oligoureas Bearing Proteinogenic Side Chains. *Angew. Chem. Int. Ed.* **2002**, *41*, 1893–1895.

(26) Kirshenbaum, K.; Barron, A. E.; Goldsmith, R. A.; Armand, P.; Bradley, E. K.; Truong, K. T. V.; Dill, K. A.; Cohen, F. E.; Zuckermann, R. N. Sequence-Specific Polypeptoids: A Diverse Family of Heteropolymers with Stable Secondary Structure. *Proc. Natl. Acad. Sci. U. S. A.* **1998**, *95*, 4303–4308.

(27) Sang, P.; Huang,B.; Xue, S.; Odom, T.; Cai, J. Sulfono-γ-AApeptides as Helical Mimetics: Crystal Structures and Applications. *Acc. Chem. Res.* **2020**, *53*, 2425–2442.

(28) Nelson, J. C.; Saven, J. G.; Moore, J. S.; Wolynes, P. G. Solvophobically Driven Folding of Nonbiological Oligomers. *Science* **1997**, *277*, 1793–1796.

(29) Bassani, D. M.; Lehn, J. M.; Baum, G.; Fenske, D. Designed Self-Generation of an Extended Helical Structure from an Achiral Polyheterocyclic Strand. *Angew. Chem. Int. Ed.* **1997**, *36*, 1845–1847.

(30) Jiang, H.; Léger, J. M.; Huc, I. Aromatic δ-Peptides. *J. Am. Chem. Soc.* **2003**, *125*, 3448–3449.

(31) Horne, W. S.; Grossmann, T. N. Proteomimetics as Protein-Inspired Scaffolds with Defined Tertiary Folding Patterns. *Nat. Chem.* **2020**, *12*, 331–337.

(32) George, K. L.; Horne, W. S. Foldamer Tertiary Structure through Sequence-Guided Protein Backbone Alteration. *Acc. Chem. Res.* **2018**, *51*, 1220–1228.

(33) Mazzier, D.; De, S.; Wicher, B.; Maurizot, V.; Huc, I. Parallel Homochiral and Anti-Parallel Heterochiral Hydrogen-Bonding Interfaces in Multi-Helical Abiotic Foldamers. *Angew. Chemie. Int. Ed.* **2020**, *59*, 1606–1610.

(34) Lombardo, C. M.; Kumar, V.; Douat, C.; Rosu, F.; Mergny, J. L.; Salgado, G. F.; Guichard, G. Design and Structure Determination of a Composite Zinc Finger Containing a Nonpeptide Foldamer Helical Domain. *J. Am. Chem. Soc.* **2019**, *141*, 2516–2525.

(35) Horne, W. S.; Price, J. L.; Keck, J. L.; Gellman, S. H. Helix Bundle Quaternary Structure from α/β-Peptide Foldamers. *J. Am. Chem. Soc.* **2007**, *129*, 4178–4180.

(36) Wang, P. S. P.; Schepartz, A. β-Peptide Bundles: Design. Build. Analyze. Biosynthesize. *Chem. Commun.* **2016**, *52*, 7420–7432.

(37) Collie, G. W.; Pulka-Ziach, K.; Lombardo, C. M.; Fremaux, J.; Rosu, F.; Decossas, M.; Mauran, L.; Lambert, O.; Gabelica, V.; Mackereth, C. D.; Guichard, G. Shaping Quaternary Assemblies of Water-Soluble Non-Peptide Helical Foldamers by Sequence Manipulation. *Nat. Chem.* **2015**, *7*, 871–878.

(38) Ferrand, Y.; Huc, I. Designing Helical Molecular Capsules Based on Folded Aromatic Amide Oligomers. *Acc. Chem. Res.* **2018**, *51*, 970–977.

(39) Seo, S. B.; Lee, S.; Jeon, H. G.; Jeong, K. S. Dramatic Enhancement of Binding Affinities Between Foldamer-Based Receptors and Anions by Intra-Receptor π-Stacking. *Angew. Chemie. Int. Ed.* **2020**, *59*, 10441–10445.

(40) Collie, G. W.; Bailly, R.; Pulka-Ziach, K.; Lombardo, C. M.; Mauran, L.; Taib-Maamar, N.; Dessolin, J.; Mackereth, C. D.; Guichard, G. Molecular Recognition within the Cavity of a Foldamer Helix Bundle: Encapsulation of Primary Alcohols in Aqueous Conditions. *J. Am. Chem. Soc.* **2017**, *139*, 6128–6137.

(41) Melicher, M. S.; Walker, A. S.; Shen, J.; Miller, S. J.; Schepartz, A. Improved Carbohydrate Recognition in Water with an Electrostatically Enhanced β-Peptide Bundle. *Org. Lett.* **2015**, *17*, 4718–4721.

(42) Yoo, S. H.; Collie, G. W.; Mauran, L.; Guichard, G. Formation and Modulation of Nanotubular Assemblies of Oligourea Foldamers in Aqueous Conditions Using Alcohol Additives. *Chempluschem* **2020**, *85*, 2243–2250.

(43) Collie, G. W.; Lombardo, C. M.; Yoo, S. H.; Pułka-Ziach, K.; Gabelica, V.; Mackereth, C. D.; Rosu, F.; Guichard, G. Crystal Structures Capture Multiple Stoichiometric States of an Aqueous Self-Assembling Oligourea Foldamer. *Chem. Commun.* **2021**, *57*, 9514–9517.

(44) Walshaw, J.; Woolfson, D. N. Extended Knobs-into-Holes Packing in Classical and Complex Coiled-Coil Assemblies. *J. Struct. Biol.* **2003**, *144*, 349–361.

(45) Lombardo, C. M.; Collie, G. W.; Pulka-Ziach, K.; Rosu, F.; Gabelica, V.; Mackereth, C. D.; Guichard, G. Anatomy of an Oligourea Six-Helix Bundle. *J. Am. Chem. Soc.* **2016**, *138*, 10522–10530.

(46) Stewart, J. J. P. Optimization of Parameters for Semiempirical Methods VI: More Modifications to the NDDO Approximations and Re-Optimization of Parameters. *J. Mol. Model.* **2013**, *19*, 1–32.

(47) Mesleh, M. F.; Hunter, J. M.; Shvartsburg, A. A.; Schatz, G. C.; Jarrold, M. F. Structural Information from Ion Mobility Measurements: Effects of the Long-Range Potential. *J. Phys. Chem.* **1996**, *100*, 16082–16086.

(48) Mecinović, J.; Snyder, P. W.; Mirica, K. A.; Bai, S.; Mack, E. T.; Kwant, R. L.; Moustakas, D. T.; Héroux, A.; Whitesides, G. M. Fluoroalkyl and Alkyl Chains Have Similar Hydrophobicities in Binding to the "Hydrophobic Wall" of Carbonic Anhydrase. *J. Am. Chem. Soc.* **2011**, *133*, 14017–14026.

(49) Fletcher, J. M.; Harniman, R. L.; Barnes, F. R. H.; Boyle, A. L.; Collins, A.; Mantell, J.; Sharp, T. H.; Antognozzi, M.; Booth, P. J.; Linden, N.; Miles, M. J.; Sessions, R. B.; Verkade, P.; Woolfson, D. N. Self-Assembling Cages from Coiled-Coil Peptide Modules. *Science* **2013**, *340*, 595–599.

(50) Sawada, T.; Matsumoto, A.; Fujita, M. Coordination-Driven Folding and Assembly of a Short Peptide into a Protein-like Two-Nanometer-Sized Channel. *Angew. Chemie. Int. Ed.* **2014**, *53*, 7228-7232.

(51) Molski, M. A.; Goodman, J. L.; Craig, C. J.; Meng, H.; Kumar, K.; Schepartz, A. β-Peptide Bundles with Fluorous Cores. *J. Am. Chem. Soc.* **2010**, *132*, 3658–3659.

(52) Marsh, E. N. G. Fluorinated Proteins: From Design and Synthesis to Structure and Stability. *Acc. Chem. Res.* **2014**, *47*, 2878–2886.

(53) Zhai, X.; Malakhova, M. L.; Pike, H. M.; Benson, L. M.; Bergen III, H. R.; Sugár, I. P.; Malinina, L.; Patel, D. J.; Brown, R. E. Glycolipid Acquisition by Human Glycolipid Transfer Protein Dramatically Alters Intrinsic Tryptophan Fluorescence. *J. Biol. Chem.* **2009**, *284*, 13620–13628.

(54) Lehn, J. M. From Supramolecular Chemistry towards Constitutional Dynamic Chemistry and Adaptive Chemistry. *Chem. Soc. Rev.* **2007**, *36*, 151–160.

TOC graphics